INSTITUTE OF PHYSICS PUBLISHING JOURNAL OF MICROMECHANICS AND MICROENGINEERING
J. Micromech. Microeng. 11 (2001) 165–174 www.iop.org/Journals/jm PII: S0960-1317(01)13669-7

An experimental study of microfabricated spark gaps: wear and erosion characteristics

Pahnit Seriburi, Dan Kercher and Mark G Allen

Microelectronics Research Center, School of Electrical and Computer Engineering, Georgia Institute of Technology, Atlanta, GA 30332, USA

Received 3 May 2000

Abstract
The objective of this work is to experimentally study the erosion and wear characteristics of microfabricated spark gaps. A microfabricated spark gap is a small-scale, low-profile ignition device that can be used, for example, for a small-scale combustion engine. Wear characteristics of this spark gap are important parameters to study to ensure long lifetime and trouble-free operation of the small-scale combustion engine. In this research, microfabricated spark gaps are made of metals—nickel, platinum, and silver—which are currently used in macro-scale spark plugs. A spark gap structure is built by microfabrication processes including photolithography, electrodeposition and screen-printing processes. The finished spark gap is then repetitively tested and optically measured for erosion and wear to determine the experimental volume erosion rate. Six experiments for observing the effects on spark erosion characteristics from six different parameters are constructed. These parameters are the spark gap distance, the electrode height and width, the spark energy, the source of spark energy, the method of fabrication, and the spark gap electrode material. It was found that all parameters except the spark gap distance affected the erosion characteristics of microfabricated spark gaps, and that the particle ejection model might be an appropriate erosion mechanism at work for these microfabricated spark gaps.

1. Introduction

Recently, there has been much interest in the potential application of small-scale combustion both for actuators and for power generation in microelectromechanical systems (MEMS) [1]. In some combustion processes, such as reciprocating devices or pulse combustors, ignition of the combustible mixture using an electrical spark at every cycle is used. Even in nonreciprocating devices, e.g., rotary engines and turbines, single sparks can be a useful way to initiate the combustion process. To be applicable to a small-scale combustion engine, instead of a typical spark ignition device or a conventional spark plug, a small-scale, low-profile electrical spark ignition device, called a 'microfabricated spark gap', is used and fabricated by MEMS technology.

The objective of this research is to experimentally study the characteristics, especially wear and erosion, of microfabricated spark gaps, and to compare the results with literature theories on erosion and wear. Wear and erosion characteristics of these spark gaps are important parameters to study to ensure long lifetime and trouble-free operation of the small-scale combustion engine. Although there is much literature on wear characteristics and erosion models of conventional arc discharge devices [2–27], because of the differing fabrication techniques and the size scales of MEMS spark gaps, these erosion characteristics should be determined on the MEMS gaps themselves.

In this paper, section 2 provides a detailed background and literature review of materials for microfabricated spark gap electrodes. In section 3, details of experimental methods and design to be used in microfabricated spark gaps assessment are presented. In section 4, a detailed outline of the experiments and their operating conditions are explained individually. These experiments have been conducted to determine the erosion characteristics as a function of six experimental parameters. These parameters are the spark gap distance, the electrode height and width, the spark energy, the source of spark energy, the method of fabrication, and the spark gap electrode material.

Section 5 presents the wear and erosion characteristic results as a function of the six experimental parameters, as well as some discussion of the results. Finally, conclusions regarding the microfabricated spark gap erosion and wear characteristics studied in this research are reached in section 6.

2. Materials for microfabricated spark gap electrodes

Spark gap materials have been carefully selected because the erosion characteristics of the spark gap depend directly on its material properties. Furthermore, it has been presented in the literature [13] that erosion rates of metals are not consistently correlated with any single mechanical property. Goretta *et al* [13] proposed that the erosion rates of ductile metals be linked with the hardness of the eroded surface, with ductility, or with thermophysical properties, such as heat capacity, thermal conductivity and the melting point of those metals. In several papers [8, 13], it has been stated that metals with high heat capacity, melting points and good oxidation resistance tend to have a better resistance to erosion. Moreover, the sputtering yield or erosion rate of a material depends on the melting point and boiling point values, which correlate with sublimation energy [8]. Engel *et al* [7] have reported that another parameter which affects the wear characteristics of spark electrodes is the morphology of the material (i.e., its microscopic structure). This is especially true for composite materials and *in situ* extruded fibre materials.

For all of the above results, when considering materials as candidates for spark gap electrodes, three important factors are the melting and boiling points of the material, the material sputtering resistance, and the oxidation characteristics of the material in combustion environments.

There is a well-developed literature on materials for conventional spark plugs [2, 8, 26]. Appropriate microfabricated spark gap materials can be determined by considering which of the conventional spark plug materials are compatible with micromachining and MEMS technology. An additional challenge in producing microfabricated spark gaps, as opposed to conventional spark plugs, is that since the total electrode volumes are low, only very small amounts of erosion can correspond to large percentage decreases in the electrodes.

In this research, nickel has been chosen as the first material to study because of its high melting point, 1452 °C [28], and well-developed fabrication processes [29]. Platinum is an interesting material to study next because of its high melting point, 1768.4 °C, and because fabrication processes for platinum are available. Moreover, platinum has been widely used for commercial conventional spark plug tips to improve corrosion resistance. The last material selected in this research work is silver. Although it has a relatively low melting point, silver is a conventional spark plug material and fabrication processes for silver are available. Therefore, it is appropriate to choose silver as one of the microfabricated spark gap materials and to compare its results with nickel and platinum.

3. Experimental methods and design

3.1. Experimental parameters

There are many parameters of the microfabricated spark gap that affect its wear and erosion characteristics. Knowledge of the dependence of wear and erosion characteristics on different gap distances, and electrode height and width, will allow the determination of an appropriate spark gap geometry which will provide good wear resistance over the micro-combustion engine life. Understanding how erosion characteristics are affected by different spark gap electrode materials and methods of fabrication will also provide an optimal fabrication process and material for microfabricated spark gaps. Awareness of how the spark energy as well as its source may affect the erosion characteristics of microfabricated spark gaps is another important and interesting factor to study.

To study the effects of these parameters on wear and erosion characteristics, six selected experiments are conducted individually for six important parameters. These parameters of interest are the spark gap distance, the electrode height and width, the spark energy, the source of spark energy, the method of fabrication, and the spark gap electrode material.

3.2. Method of fabrication

Conventional thin-film micromachining approaches, where the deposited film thicknesses are of the order of microns, may not be appropriate for spark gap materials, as erosion will cause a much larger percentage of material to be removed with each spark cycle, quickly rendering the spark gaps inoperative. Instead, MEMS-compatible procedures that result in thick deposited films should be used. Two attractive techniques that satisfy this criterion are electrodeposition (electroplating) and screen-printing. In this research, a low-profile and small-scale spark gap structure is built using both of these technologies. Spark erosion results from these two techniques will be compared.

3.2.1. Electrodeposition technique. Nickel has been chosen as the electroplated spark gap material due to the fact that nickel plating processes for MEMS are well-developed [29]. The micro spark gaps are fabricated using a one-mask photolithographic process on glass substrates. A polymer mold is photodefined using this mask. Then, the designated material, nickel, is electrodeposited in the polymer mold.

First, a Cr/Cu/Ti, electroplating seed layer, 500/2000/500 angstroms in thickness, is deposited on a glass substrate using electron-beam evaporation. Second, a photosensitive polymer (AZ 4620) is spin-cast to the desired thickness, about 20–80 microns, and photodefined to form molds for the spark gap structures. The top Ti layer is then removed and the spark gap structures are electroplated with the desired metal through the mold in a standard plating bath. To achieve smooth-surfaced nickel structures at a metal deposition rate of 5 microns per hour, a current density of 5 mA cm^{-2} is used in a standard Watts Ni plating bath [29]. After electroplating, acetone is used to remove the AZ 4620 mold structures. Then, the uncovered seed layer, which consists of Ti and Cu layers on top of a Cr layer, is removed, leaving behind the completed spark plugs.

3.2.2. Screen-printing technique. Three materials have been selected for the screen-printed electrodes. The first material is nickel, so that direct comparisons can be made between the electroplated and screen-printed electrode materials. The other two materials, silver and platinum, have been selected as they are commonly used in either arcing environments (silver/silver oxides) or in actual spark gaps in automotive and other internal combustion applications (platinum).

In the screen-printing process, the desired metal ink is screen-printed through a patterned mask or a screen onto a glass substrate, baked, and fired. All inks have been obtained from Dupont (part nos. 6142D, 9538, and 9141).

Typical firing temperatures and times for different materials are listed below.

Ag	0–500 °C at 5 °C/min, hold for 30 min 500–850 °C at 5 °C/min, hold for 30 min
Pt	0–500 °C at 5 °C/min, hold for 30 min 500–900 °C at 5 °C/min, hold for 30 min
Ni	0–300 °C at 5 °C/min, hold for 30 min 300–590 °C at 5 °C/min, hold for 30 min

3.3. Source of spark energy

3.3.1. Dual transformer approach. The first spark ignition testing system studied in this research uses a dual transformer approach. The first transformer (special ferrite transformer) is used to increase the voltage to about 340 V. The secondary of this transformer is connected to a bank of capacitors and diodes. The capacitors are charged to the desired energy, and when triggered by the SCR switch, the stored energy in the capacitors is dumped to the second transformer. The second transformer (25 kV pulse transformer) can increase the voltage up to about 20 kV, which is used as a high-voltage pulse to jump the arc across the gap of the spark plug. The SCR switch is triggered by a TTL pulse from the 3310A function generator (Hewlett Packard) at a rate of 20 Hz, and results in 20 Hz spark pulses at the spark gap.

If losses in the second transformer can be neglected, the energy in the spark can be set by the energy stored in the capacitor bank. This capacitor energy is determined by the charge stored in this bank of capacitors. Assuming the capacitors are linear, equation (1) below expresses the energy stored in the capacitor, where E represents the energy, C represents the capacitance and V represents the voltage across the capacitor.

$$E = 0.5CV^2. \tag{1}$$

The theoretical minimum ignition energy for stochiometric mixtures of propane and air is 0.31 mJ [28]. Additional energy is often required to initiate combustion as a result of electrical losses, heat losses, and electrode oxidation. Therefore, in this research, the testing energies are set at 5 and 10 mJ, which correspond to a charging voltage of 340 V and capacitance values of 81.6 and 163 nF, respectively. However, actual commercial-value capacitances used in this circuit are 82 and 168 nF. It has been reported in the literature [30–31] that this approach can result in very low energy transfer efficiency, 1% or less. Most of the energy is lost in the transformer that is connected to the spark gap and in the spark gap wire. Therefore, it is difficult to determine the exact energy supplied to the spark gap itself.

3.3.2. High voltage capacitor approach. Because of the difficulty of accurate energy assessment in the transformer approach, an alternative approach based on the direct discharge of a high voltage capacitor was developed. In this research, a high voltage amplifier model 609A from Trek Inc. is used to supply the high voltage signal. This high voltage amplifier has a gain of 1000 and a maximum output of 10 kV. The input to this high voltage amplifier is a programmable function generator (Phillip). In order to make a spark pulse every 50 ms (20 Hz), the function generator is set to a square wave with frequency of 20 Hz and a duty cycle of 4–6% at a peak voltage of 6–8 V. Power from this amplifier is supplied to the connecting RC circuit to charge the capacitor. It is better to attach another high voltage capacitance, 332 pF, between the high voltage amplifier output and RC circuit to isolate the external action from the amplifier. The voltage across the capacitors, or also across the spark gap, is slowly ramping up with a known time constant, $\tau = RC$, where R is the resistance and C is the capacitance. At the moment that the voltage across the spark gap reaches the breakdown voltage, the spark jumps across the gap.

Assuming that the time constant of the RC circuit is much longer than the spark period, the energy in the spark can be set by the capacitance of the capacitor and the voltage across the gap at the inception of the spark. In this paper, a 20 MΩ resistance and 48.5 pF capacitance, which will give a time constant of about 1 ms, are used. Compared to the spark duration (which is of the order of microseconds), the energy that is supplied to the spark can be assumed to be equal to the energy stored in the 48.5 pF capacitor. The expression of equation (1) is used to calculate this energy. For 2 mm microfabricated spark gaps, the breakdown voltage in air ranges experimentally from 3.75 to 5.5 kV. Because the capacitor does not completely discharge, but instead its voltage drops suddenly from the breakdown voltage to a measured voltage of 1.25 kV and then recharges again, equation (1) must be modified to equation (2). Equation (2) replaces 'V^2' in equation (1) by '$V_H^2 - V_L^2$', where V_H represents the upper bound of capacitor voltage and V_L represents the lower bound of capacitor voltage:

$$E = 0.5C\left(V_H^2 - V_L^2\right). \tag{2}$$

Therefore, with $V_H = 3.75$–5.5 kV, $V_L = 1.25$ kV, $C = 48.5$ pF, the spark energy in this approach will range from 303 to 695 micro joules (μJ). The actual spark energy may be more than that reported here because of the additional current from the high voltage amplifier that can be delivered to the spark gap; however, because of the long time constant of charging the discharge capacitor, this current is assumed to be negligible.

It is noted that to measure the breakdown voltage, a resistive voltage divider is used. Series connected resistors (100 MΩ + 400 kΩ) are connected parallel to the spark gap and a voltage across the small resistor (400 kΩ) is measured using a TDS 220 oscilloscope (Tektronix). This allows the measurement of V_H and V_L for equation (2).

3.4. Erosion assessment

3.4.1. Quantitative erosion measurement: erosion rate. In this paper, for erosion and wear optical measurement, an optical microscope (Nikon) is used to measure heights, widths and removal lengths of both sides of spark electrodes after the spark gap has been run for a specific number of spark cycles. The multiplication of these width and removal length values provides removal areas of the spark gap. Then, a volume removal or volume erosion is calculated by multiplying removal areas by the height of the spark gap. By plotting many values of volume erosion as a function of the number of spark cycles, a volume erosion graph can be obtained. The volume erosion rate is simply the slope of the graph. The unit of volume erosion rate is cubic micron per cycle.

3.4.2. Qualitative erosion measurement: surface erosion characteristics. Although the optical microscope measurement method described above yields quantitative information about erosion rate, additional information regarding the erosion mechanism can be obtained by a detailed study of the surface morphology of the spark gap materials. This is best done by observation in a scanning electron microscope (SEM) (Hitachi). By using this tool, it may be possible to determine not only the structure of the electrode surface after sparking, but also to study the pattern of ejected material from the electrode surface that has redeposited on the glass. From these measurements, a qualitative comparison to literature theories of wear and erosion can be made.

4. Detailed outline of experiments

The six parameters of interest studied in this research are the spark gap distance, the electrode height and width, the spark energy, the source of ignition energy, the method of fabrication, and the spark gap electrode material. Both qualitative and quantitative measurements are chosen to determine wear and erosion characteristics of microfabricated spark gaps affected by these parameters. The microfabricated spark gaps are tested and a volume removal for each spark gap is optically measured repetitively up to 1 million spark cycles or until spark gaps run inconsistently. By using the quantitative optical measurement, an experimental volume erosion rate can be determined. Also, after the erosion test, the spark gaps are examined qualitatively in an SEM to observe the surface morphology of the spark gap materials.

Six selected experiments are conducted in this study. Erosion characteristics affected by different spark gap distances are investigated in experiment 1. Two spark gap distances, a 175 micron gap and a 2 mm gap, are used in this experiment. In experiment 2, the effect of different electrode heights and widths on erosion characteristics will be studied. Two 175 micron spark gaps that differ in height are tested. Also, two sets of 2 mm spark gaps with a difference in height and width are assessed. In experiment 3, six spark gaps are tested at two different spark energies, 5 and 10 mJ, to observe the influence of spark energy on erosion characteristics. In experiment 4, both spark ignition circuits, the dual transformer approach and the high voltage capacitor approach, are used to run four spark gaps. This will determine erosion characteristics as a function of the source of spark energy. Erosion characteristics as a function of the method of fabrication are studied in experiment 5. Both the electrodeposition and screen-printing processes are chosen to fabricate all spark gaps in this experiment and the results on wear and erosion characteristics from both techniques will be compared. Finally, in experiment 6, three different materials (nickel, platinum and silver) are chosen as screen-printed spark gap electrode materials, to study how erosion characteristics are affected by electrode materials. Each of these parameters of interest and its experimental details are presented and described here.

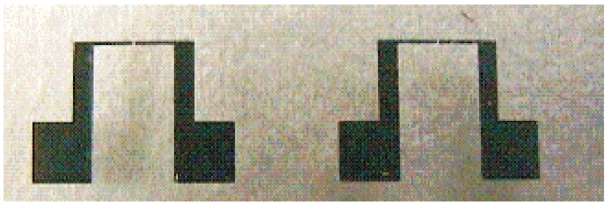

Figure 1. Small gap (175 micron) spark gap.

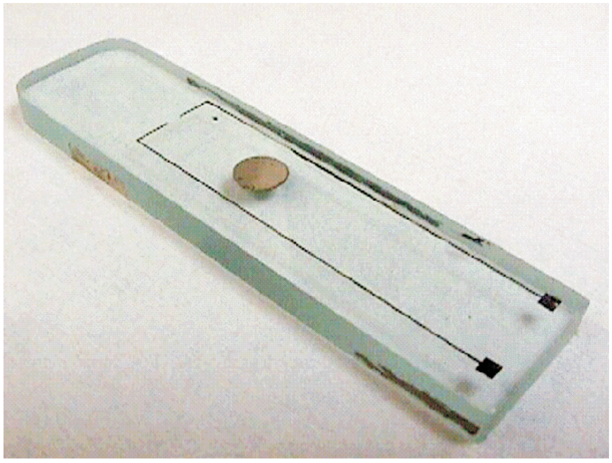

Figure 2. Large gap (2 mm) spark gap.

4.1. Experiment 1: spark gap distance

The first spark gap structure is a simple two-electrode system with a 175 micron arc gap (figure 1). This is an arbitrary gap distance designed to test the wear of spark gaps by keeping both ends of the spark gap within the field of view of a single microscope objective. The electrodes are nominally 205–225 microns wide by 40 microns high to produce a sample of a sufficient volume to enable extended wear data to be gathered.

The second spark gap geometry is designed with a larger gap of 2 mm (figure 2). A combustion experiment indicated that a 2 mm gap distance was an appropriate gap for repetitive and reliable ignition of propane–air mixtures. The electrodes of this device are nominally 230–250 microns wide. The height of this device is varied between 60 and 80 microns.

Both 175 micron and 2 mm spark gaps are fabricated using the same material (nickel), and the same fabrication process (electrodeposition). All spark data are gathered in laboratory air using the dual transformer approach. The ignition circuit is triggered with a 20 Hz pulse signal, resulting in 20 Hz spark

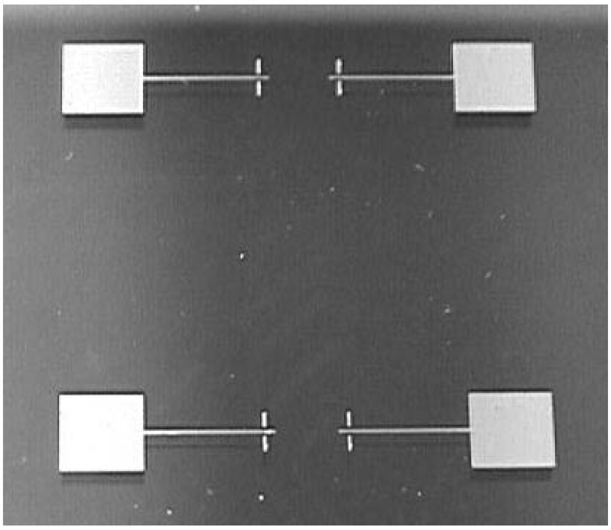

Figure 3. Small 2 mm spark gaps.

pulses at the spark gap. All spark gaps are tested up to 1.5 million spark cycles. For 175 micron spark gaps, one spark gap is tested with 5 mJ energy and the other is tested with 10 mJ energy. For 2 mm spark gaps, two samples are tested with 5 mJ energy and the other two are tested with 10 mJ energy.

4.2. Experiment 2: electrode height and width

To assess the effect of electrode height and width on erosion characteristics, electrodes of two different heights and widths, with gap lengths of 175 micron and 2 mm have been designed and built using the same material (nickel) and the same electrodeposition process. All spark gaps in experiment 2 are tested in laboratory air with the dual transformer approach at the calculated 10 mJ energy. All spark gaps are tested up to 1.5 million spark cycles at a 20 Hz spark pulse rate.

For the 175 micron length spark gaps (figure 1), two heights, one 40 microns and the other 160 microns, are tested. For the 2 mm length spark gaps, four test structures are used. The first two electrodes are designed as presented earlier in figure 2. The second two electrodes are designed to have a much smaller electrode size, 100 microns wide by 20 microns high, as shown in figure 3.

It is noted that these smaller 2 mm spark gaps also have reference lines next to the spark electrodes. These lines are located 250 microns away from the tip. These lines are used as a reference point in measuring the removal lengths. As a result, it is believed that this new design will provide a better and more accurate technique in measuring electrode removal lengths.

4.3. Experiment 3: spark energy

The effect of varying spark energy on wear and erosion characteristics is another interesting parameter to study. Two spark energies, 5 mJ and 10 mJ, are used for this experiment. All spark gaps use the same electrode material (nickel) and the same fabrication process (electrodeposition). The dual transformer approach is used as a source of spark energy. All spark data are gathered in laboratory air and tested up to 1.5 million spark cycles (20 Hz spark pulse). Two 175 micron spark gaps (figure 1), and four 2 mm spark gaps are investigated (figure 2).

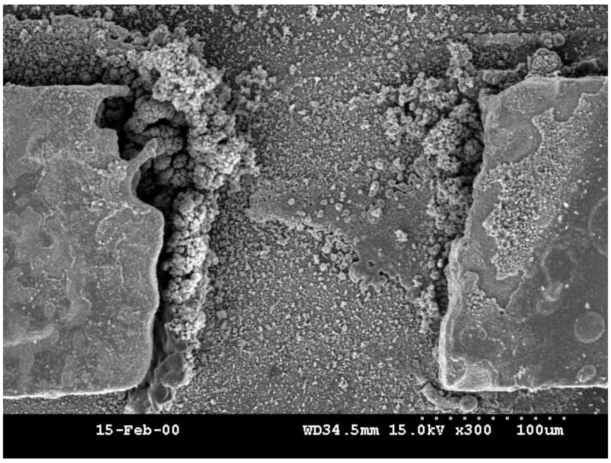

Figure 4. An SEM micrograph of tips of the 175 micron spark gap electrode in experiment 1.

4.4. Experiment 4: source of spark energy

A difference in source of ignition energy can also affect the wear and erosion characteristics of spark gaps, according to the literature [6]. In this experiment, a nominal energy of 10 mJ for both sources of ignition energy has been attempted. To obtain the 10 mJ energy from the high voltage capacitor approach, a relatively high capacitance value of 1000 pF must be used. However, because there is a very high current discharge when using this large capacitor in the high voltage capacitor approach, a 20 Hz spark pulse cannot be obtained continuously using the available equipment. Spark gaps are therefore tested using a lower energy (in the hundreds of μJ range) when using the high voltage capacitor approach. With the dual transformer approach, energy is held at a nominal 10 mJ level (although actual energies are lower due to losses inherent in this topology).

Two 2 mm spark gaps are tested with a dual transformer approach. The other two 2 mm spark gaps are tested with a high voltage capacitor approach. All tests are run in laboratory air at a spark rate of 20 Hz. All spark gaps are built with the same electrode height and width using the same electrode material (nickel), and the same electrodeposition technique. All spark data are gathered up to 1 million spark cycles.

4.5. Experiment 5: method of fabrication

Nickel spark gaps fabricated by both the electrodeposition and screen-printing techniques are compared. The gap distance for these spark gaps is 2 mm. Every spark gap is tested at 10 mJ spark energy as supplied by the dual-transformer ignition circuit. All spark data are gathered in laboratory air up to 1 million spark cycles. The nickel electroplated spark gap electrodes are 100 microns wide by 20 microns high. The nickel screen-printed spark gap electrodes are 300–350 microns wide by 35 microns high.

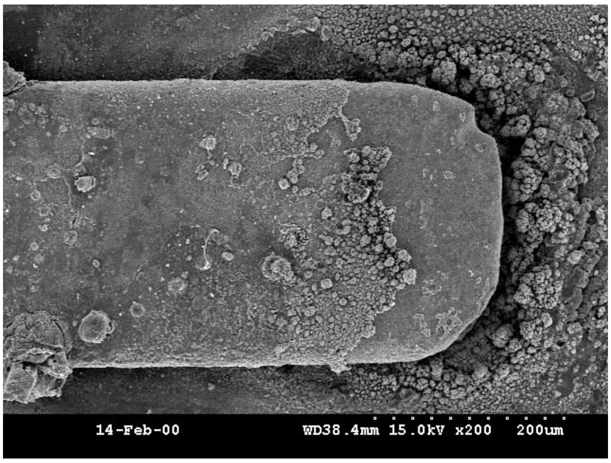

Figure 5. An SEM micrograph of the cathode tip of the 2 mm electroplated nickel spark gap electrode in experiment 1.

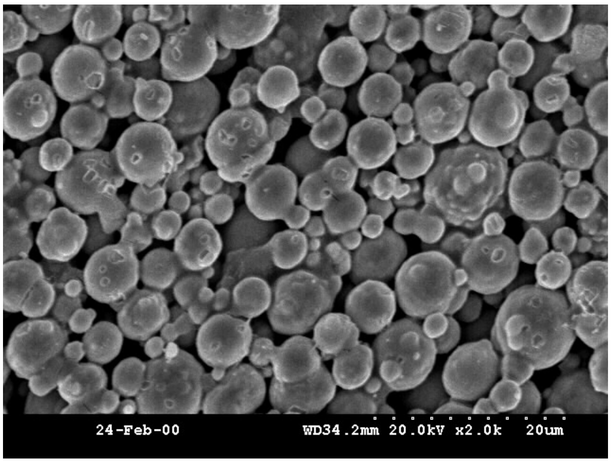

Figure 6. An SEM micrograph of the original surface of the screen-printed nickel spark electrode.

4.6. Experiment 6: spark gap electrode material

In this research, nickel, platinum, and silver have been chosen as screen-printed spark gap electrode materials to study the effect of material on erosion. Two nickel, two silver, and three platinum screen-printed spark gaps are fabricated using the screen-printing technique. Spark gap electrodes are nominally 200–350 microns wide by 5–35 microns high. Variations in the width and height of these spark gap electrodes are mainly due to different screen-printed metal ink properties for different materials. All spark gaps are tested at 10 mJ with a dual transformer approach circuit at a rate of 20 Hz spark pulse. All spark data are gathered in laboratory air up to 1 million spark cycles.

5. Results and discussion

5.1. Experiment 1: spark gap distance

Volume erosion data are plotted as a function of the number of spark cycles and an experimental volume erosion rate as a function of spark cycles is equal to the slope of the graph. For 175 micron spark gaps, the volume erosion rate is equal to 0.04 cubic micron/cycle in 5 mJ case and 0.14 cubic micron/cycle in 10 mJ case. For 2 mm spark gaps, the volume erosion rate is equal to 0.05 ± 0.01 cubic micron/cycle in the 5 mJ case and 0.23 cubic micron/cycle in the 10 mJ case.

It is observed that the higher the number of spark cycles is, the higher the value of the volume removal. Moreover, there is not much difference in the erosion rate when spark gaps are of a different gap distance for both 5 and 10 mJ spark energies. Therefore, it is assumed that the erosion characteristics of the spark gaps in experiment 1 operating conditions are independent of the spark gap distance. From SEMs obtained from an optical microscope, the longer the period of time the spark gap devices are run, the rounder the electrodes are. This is because the electric field between the electrodes is higher at the sharp edges so that the spark tends to jump to and from those sharp points more than other areas. This results in more erosion at those sharp edges. This effect has also been reported in the literature [2]; a metal removal of spark gaps manifests itself by a rounding of the electrode edges, which widens the spark gap. Furthermore, figures 4 and 5 show SEM images for both 175 micron and 2 mm spark gaps. Both pictures appear similar in the sense that both show the particles depositing around the tip of each electrode. Also, they both illustrate the similar melting-like damaged surfaces at the tip for the 175 micron and the 2 mm spark gaps. It is believed that the erosion mechanism for all spark gaps in this experiment is the same and that the difference in gap distance does not affect the erosion mechanism.

5.2. Experiment 2: electrode height and width

Volume erosion data are plotted as a function of the number of spark cycles and an experimental volume erosion rate as a function of spark cycles is equal to the slope of the graph. For 175 micron spark gaps, the volume erosion rate is equal to 0.18 cubic micron/cycle in the thicker electrode case and 0.14 cubic micron/cycle in the thinner electrode case. For 2 mm spark gaps, the volume erosion rate is equal to 0.23 cubic micron/cycle in the larger and thicker electrode case and 0.6 ± 0.1 cubic micron/cycle in the smaller and thinner electrode case.

In the 175 micron spark gap case, there is not much difference in the volume erosion rate for two spark gaps that differ in height. However, with the same volume erosion rate, but a difference in height, the removal lengths of those two samples are different. When SEM images of these two spark gaps are observed, their erosion appearances are different. It is observed that the thicker the spark gap is, the shorter the removal length and the less particle deposition around the spark gap electrode. For the thinner spark gap, its removal length is greater, and more particles are sputtered around the electrodes.

In the 2 mm spark gap case, a large difference in the volume removal rate can be observed for two spark gap electrodes that differ in height and width. The smaller electrode spark gap has a much higher erosion rate compared to the larger one. It has been reported in the literature [3, 8, 26] that the smaller the electrodes are, the higher the erosion rate. This is because smaller electrodes receive a higher spark energy concentration than larger ones.

Comparing the 2 mm and the 175 micron spark gap results, it is unclear why the effects of electrode height and width on

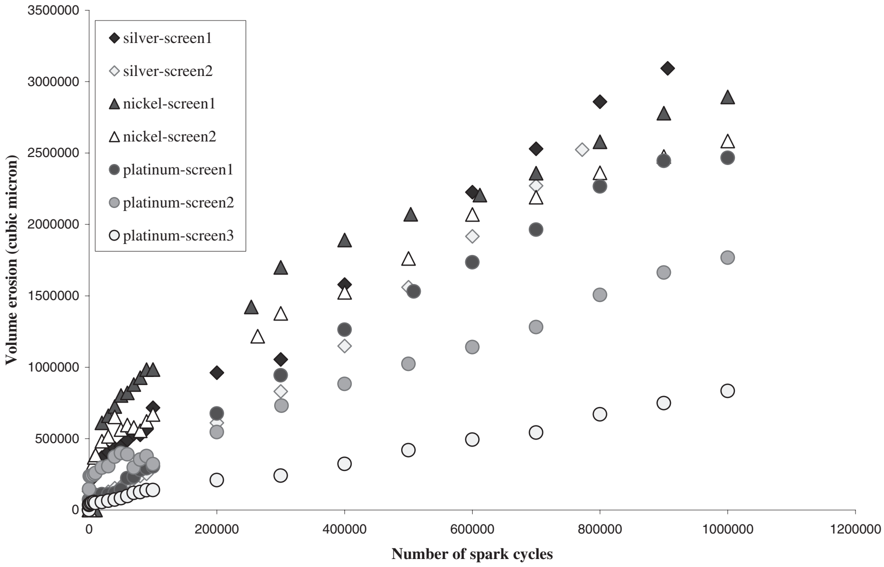

Figure 7. Volume erosion versus number of spark cycles for all spark gaps in experiment 6.

wear and erosion characteristics for both cases are different. In the 175 micron case, there is not much difference in the volume erosion rate for two samples that differ in height, but in the 2 mm spark gap case, a large difference in the volume removal rate can be observed. There are several factors that might influence the results for both cases in experiment 2. Firstly, instead of the five volume erosion data points taken for all other spark gaps, 24 data points are taken in the smaller 2 mm spark gap case. The more volume erosion data points obtained, the more accurate the calculated volume erosion rate will be. Therefore, the calculated volume erosion rate in this smaller 2 mm spark gap case may be more accurate than those of other spark gap cases. Secondly, an optical assessment technique used in the smaller 2 mm spark gap case is slightly different from those of other spark gaps. It has been noted earlier that a reference line has been added to this smaller 2 mm spark gap design to obtain a more accurate measurement. Therefore, instead of using the electrode tip as a reference point to measure the removal lengths, the additional reference line in the smaller 2 mm spark gaps is used as a new reference point. Thirdly, it is possible that a change in the electrode height (175 micron case) does not affect the erosion rate as much as a change in both electrode width and height (2 mm case).

5.3. Experiment 3: spark energy

Volume erosion data are plotted as a function of the number of spark cycles and an experimental volume erosion rate as a function of spark cycles is equal to the slope of the graph. In the 5 mJ energy case, the volume erosion rate of the 175 micron spark gaps is equal to 0.04 cubic micron/cycle and that of the 2 mm spark gaps is equal to 0.05 ± 0.01 cubic micron/cycle. In the 10 mJ energy case, the volume erosion rate of the 175 micron spark gaps is equal to 0.16 ± 0.02 cubic micron/cycle and that of the 2 mm spark gaps is equal to 0.23 cubic micron/cycle.

The erosion rate for two different spark energies can be easily distinguished. The higher the spark energy is, the higher the erosion rate. This is true for both 175 micron and 2 mm spark gaps. Also, similar wear characteristics, such as the rounding of electrodes and particle deposition around the electrodes, are found for both 5 and 10 mJ; however, the severity of the erosion is less in the 5 mJ case.

5.4. Experiment 4: source of spark energy

A linearized volume erosion rate as a function of spark cycles for every spark gap is calculated. It is found that the value of the volume erosion rate of spark gaps using a high voltage capacitor approach (0.6 ± 0.07 cubic micron/cycle) is the same as that of the volume erosion rate of spark gaps using the dual transformer approach (0.6 ± 0.1 cubic micron/cycle).

It is interesting that the volume erosion rate for both spark ignition circuits is the same although the calculated spark energies in both cases are very different. As a result, it is believed that there is much loss associated with the dual transformer approach. The actual energy applied to the spark gap is likely to be much lower than the calculated 10 mJ energy. These losses might be due to losses in the pulse transformer and electrical losses in diodes and the SCR switch.

5.5. Experiment 5: method of fabrication

A linearized volume erosion rate as a function of spark cycles for every spark gap is calculated. For the nickel electroplated spark gaps, the volume erosion rate is equal to 0.6 ± 0.1 cubic micron/cycle. For the screen-printed nickel spark gaps, the volume erosion rate is equal to 2.7 ± 0.15 cubic micron/cycle.

It has been noticed that screen-printed nickel spark gap erosion rate is much higher than that of the electroplated nickel one. An SEM micrograph of the original surface of screen-printed nickel spark gap reveals that the original nickel surface is porous (figure 6). On the other hand, the original surface of electroplated nickel is not porous. This porous property is assumed to be the major reason for the above result. Also, nickel spark gaps fabricated from the screen-printing technique are made from metal ink, which consists of nickel particles

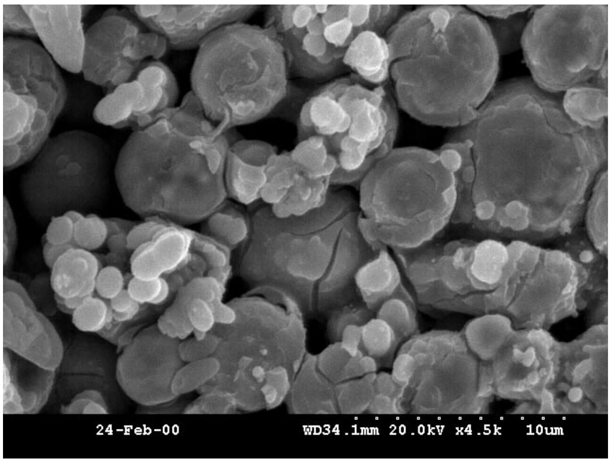

Figure 8. An SEM micrograph of the surface of the screen-printed nickel spark electrode after testing.

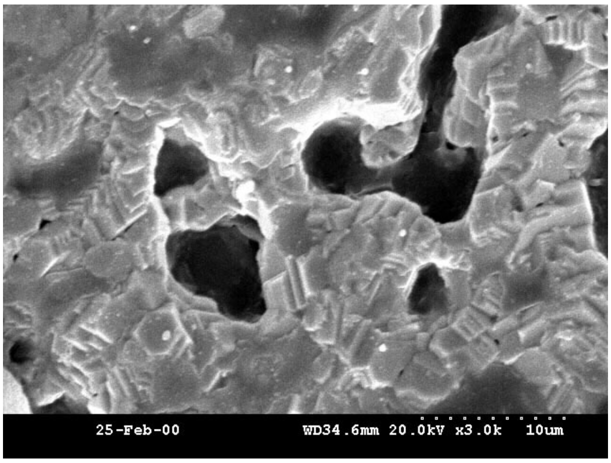

Figure 9. An SEM micrograph of the original surface of the screen-printed silver spark electrode.

suspended in an organic binder, which might also affect the erosion rate of screen-printed nickel spark gaps.

5.6. Experiment 6: spark gap electrode material

Volume erosion data are plotted as a function of the number of spark cycles and an experimental volume erosion rate as a function of spark cycles is equal to the slope of the graph (figure 7). For nickel spark gaps, the volume erosion rate is equal to 2.7 ± 0.15 cubic micron/cycle. The volume erosion rate of silver spark gaps is equal to 3.2 ± 0.5 cubic micron/cycle. For platinum spark gaps, the volume erosion rate is equal to 1.6 ± 0.8 cubic micron/cycle.

It is observed that platinum screen-printed spark gaps show the best wear resistance among the three different screen-printed materials and that silver spark gaps show the least wear resistance. These result agree well with the literature [8, 24], which has stated that materials with a higher melting point should show a better erosion resistance.

SEM micrographs reveal the changes in the spark gap surface after testing (figures 6, 8–12) compared to the original surface. From these images, it is observed that silver has the most porous surface of all three materials. This might be another reason why silver shows the least wear resistance. Although the nickel screen-printed spark gap surface is denser than the platinum surface, the erosion rate of nickel spark gaps is still higher than that of platinum spark gaps. This shows that the erosion rate of these spark gaps depends strongly on the melting point property of materials.

5.7. Erosion mechanism

From SEM micrographs (figures 13 and 14), similar surface erosion characteristics between microfabricated spark gaps and those in the literature [15] can be noticed. There is melt-like damage on the spark gap surface and also many small deposited particles around the electrodes. Therefore, it is believed that the 'particle ejection model' might be the most appropriate mechanism for microfabricated spark gaps.

Also, the supplied voltage (1–10 kV) in this work falls into the same range as that of the particle ejection model value (50 V–1 kV). If a peak spark current is determined by a

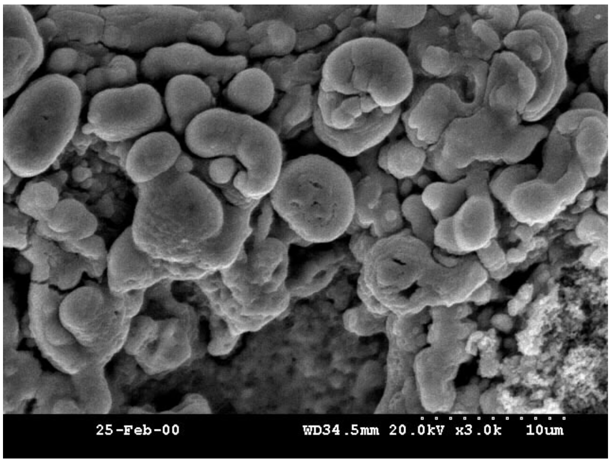

Figure 10. An SEM micrograph of the surface of the screen-printed silver spark electrode after testing.

capacitor discharge current, a spark current can be calculated using an expression in equation (3). From equation (3), the capacitor current (I) is equal to the capacitance multiplied by the derivative of the voltage (V) across the spark gap with respect to time (t). Approximating the derivative by finite values, and noting that $C = 48.5$ pF, ΔV is about 4 kV, and Δt is around 10 μs, the spark current is approximately 20 mA:

$$I = C\frac{\mathrm{d}V}{\mathrm{d}t} \approx C\frac{\Delta V}{\Delta t}. \qquad (3)$$

Therefore, the range of current in this research also falls into the same range as that of the particle ejection model.

6. Conclusion

In this research, microfabricated spark gaps have been successfully fabricated and tested. Section 3 provides details of experimental parameters and experimental methods. Then, a detailed outline of experiments is described in section 4. Both qualitative and quantitative measurements are done and the results are presented and compared with literature results in section 5. Conclusions from the wear and erosion

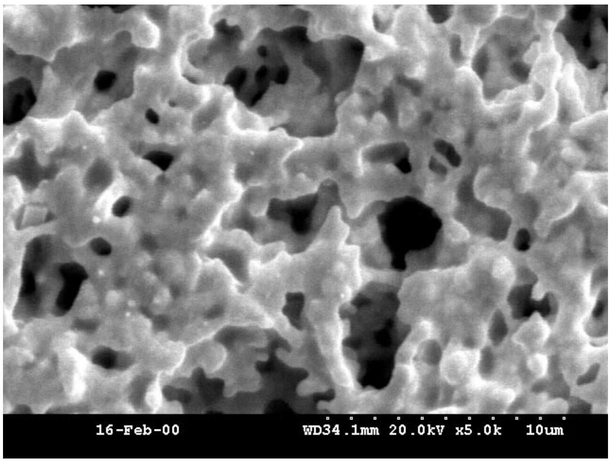

Figure 11. An SEM micrograph of the original surface of the screen-printed platinum spark electrode.

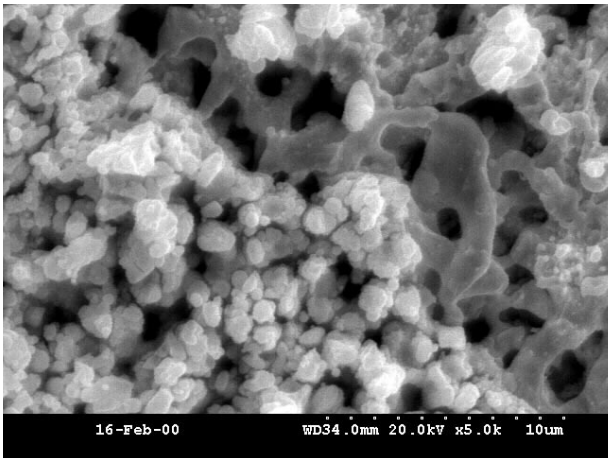

Figure 12. An SEM micrograph of the surface of the screen-printed platinum spark electrode after testing.

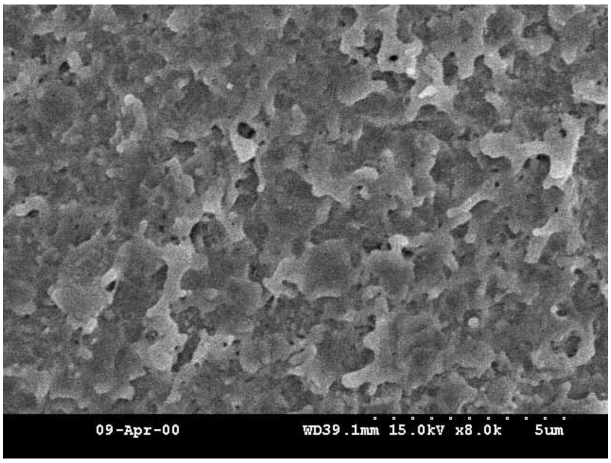

Figure 13. An SEM micrograph of the surface of the nickel electroplated spark electrode after testing.

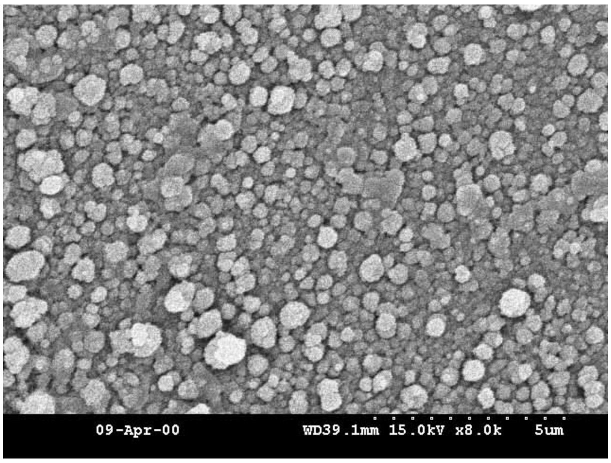

Figure 14. An SEM micrograph of deposited particles on a glass substrate between two nickel electroplated spark electrodes after testing.

characteristic results are as follows. From SEM micrographs (figures 13 and 14), similar surface erosion characteristics between microfabricated spark gaps and those in the literature [15] are observed. There is melt-like damage on the spark gap surface and there are also many small particles around the electrodes. Therefore, it is believed that the 'particle ejection model' might be the most appropriate erosion mechanism for microfabricated spark gaps. Also, the spark voltage (1–20 kV) and the spark current (20 mA) in this research are in the same range as that in the particle ejection model in the literature [15].

From the six experiments described in section 4, many interesting results are obtained.

(1) In experiment 1, there is a slight difference between the erosion characteristics of small-gap-distance and those of large-gap-distance spark gaps. It is believed that the erosion mechanism for all spark gaps in this experiment is the same and the difference in gap distance does not affect the erosion mechanism.
(2) From experiment 2, smaller electrode spark gaps provide a higher erosion rate than larger electrode spark gaps. This result is the same as those reported in the literature [3, 8, 26]. Although in the 175 micron gap case, there is no difference between two spark gaps with a difference in height, it is believed that this might be due to the fact that changing the height of the electrodes does not affect the erosion rate as much as changing both the width and height (in the 2 mm gap case). Also, the difference in erosion assessment as discussed earlier can be another reason for the above observation.
(3) In experiment 3, it is obvious that the erosion rate in the larger energy case is higher than that in the smaller energy case for both the 175 micron and 2 mm spark gaps.
(4) A similar value of the erosion rate from experiments using two different sources of ignition energy are observed although the calculated energies supplied from those two sources of spark energy are not the same. It is believed that there is much loss associated with the spark ignition circuit using a dual transformer approach. The losses in the circuit might come from losses in the pulse transformer, diodes and the SCR switch.
(5) It is believed that the spark gap erosion rate could also be affected by using different methods of spark gap fabrication. This is because different fabrication techniques cause a difference in the material properties

of spark gap structures. The screen-printing process provides a more porous spark gap surface and, as a result, a higher erosion rate is obtained.

(6) From experiment 6, similar results as in the literature are found. It has been reported that materials with higher melting points tend to have a better wear resistance [8, 13, 24]. In this experiment, platinum is the best among the three materials, followed by nickel, and then silver.

In this research, the effects of six important parameters on wear and erosion characteristics of microfabricated spark gaps have been investigated. An optimal microfabricated spark gap material and geometry can be determined based on this study. For good wear and erosion characteristics, a nickel microfabricated spark gap should be fabricated using the electrodepositon method rather than the screen-printing method. However, if the screen-printing technique is chosen for other reasons (such as ease of fabrication), platinum should be selected as a spark electrode material.

Acknowledgments

This work was supported by the Microsystems Technology Office of the Defense Advanced Research Projects Agency of the United States, under contract DABT63-98-1-0009. Microfabrication was carried out in the Georgia Technology Microelectronics Research Center, with the assistance of the staff. The authors would like to thank Jin Woo Park, Michael Fonseca, and Martin von Arx for their support as well as many meaningful technical discussions. Also, the authors would like to thank other members in the microcombustion project for many good suggestions.

References

[1] Epstein A H *et al* 1997 *9th Int. Conf. on Solid State Sensors and Actuators (Transducers'97, Chicago)* pp 753–6

[2] Meyer F *et al* 1988 *Automotive Electric/Electronic Systems* (Stuttgart: Bosch)

[3] Donaldson A L, Kristiansen M, Watson A, Zinsmeyer K and Kristiansen E 1986 *IEEE Trans. Magn.* **MAG-22** 1441

[4] Lehr M F and Kristiansen M 1989 *IEEE Trans. Plasma Sci.* **17** 811

[5] Donaldson A L and Krinstiansen M 1991 *Digest of Technical Papers, 8th IEEE Int. Conf. on Pulse Power* pp 874–7

[6] Prucker U 1998 *Proc. 18th Int. Symp. on Discharge and Electrical Insulation in Vacuum* vol 1, p 398

[7] Engel T G, Wester S L and Kristiansen M 1995 *IEEE Trans. Magn.* **31** 709

[8] Nishio K, Oshima T and Ogura H 1994 *Int. J. Vehicle Design* **15** 119

[9] Reddy R M, Cupschalk S G, Molen G M and Kuhlman J M 1985 *Digest of Technical Papers, 5th IEEE Conf. on Pulsed Power* pp 461–4

[10] Donaldson A L, Kristiansen M, Krompholz H and Hagler M O 1985 *Digest of Technical Papers, 5th IEEE Conf. on Pulsed Power* pp 457–60

[11] Felsner P, Stetter M, Hartmann W, Linsenmeyer A, Christiansen J and Frank K 1994 *J. Appl. Phys.* **76** 5661

[12] Gortler A, Schwandner A, Christiansen J and Frank K 1993 *IEEE Trans. Plasma Sci.* **21** 516

[13] Goretta K C, Arroyo R C, Wu C T and Routbort J L 1991 *Wear* **147** 145

[14] Watson A, Donaldson A L, Ikuta K and Kristiansen M 1986 *IEEE Trans. Magn.* **22** 1799

[15] Gray E W and Pharney J R 1974 *J. Appl. Phys.* **45** 667

[16] Donaldson A L, Garcia D, Kristiansen M and Watson A 1986 *IEEE Conf. Record of the 1986 17th Power Modulator Symp.* pp 146–8

[17] Young C T and Grimes D A 1978 *SAE Technical Paper Series* 780330

[18] Chen Z-K 1998 *IEEE Trans. Compon. Packag. Manuf. Technol.* A **21** 310

[19] Chen Z-K 1994 *IEEE Trans. Compon. Packag. Manuf. Technol.* A **17** 61

[20] Chen Z-K and Sawa K 1994 *J. Appl. Phys.* **76** 3326

[21] Chen Z-K and Sawa K 1993 *IEEE Trans. Compon. Hybrids Manuf. Technol.* **16** 211

[22] Wingert P C and Leung C-h 1987 *IEEE Trans. Compon. Hybrids Manuf. Technol.* **10** 56

[23] Wang B-J, Saka N and Rabinowicz E 1991 *IEEE Trans. Compon. Hybrids Manuf. Technol.* **14** 374

[24] Wang B-J, Saka N and Rabinowicz E 1992 *Wear* **157** 31

[25] Wang B-J and Saka N 1996 *Wear* **195** 133

[26] Osamura H *et al* 1999 *SAE Technical Paper Series* 1999-01-0796

[27] Wang K and Wang Q 1991 *IEEE Trans. Compon. Hybrids Manuf. Technol.* **14** 293

[28] Weast R C and Selby S M 2000 *CRC Handbook of Chemistry and Physics* (Cleveland, OH: Chemical Rubber Company)

[29] Lowenheim F A 1974 *Modern Electroplating* (New York: Wiley)

[30] Rohwein G J 1997 *IEEE Trans. Plasma Sci.* **25** 306

[31] Rohwein G J, Babcock S R and Buttram M T 1995 *Digest of Technical Papers, 10th IEEE Conf. on Pulsed Power* vol 1, p 40